NASA Technical Memorandum 87257

Undercooled and Rapidly Quenched Ni-Mo Alloys

S.N. Tewari and T.K. Glasgow
Lewis Research Center
Cleveland, Ohio

APR 1986
RECEIVED
NASA STI FACILITY

NASA

UNDERCOOLED AND RAPIDLY QUENCHED Ni-Mo ALLOYS

S.N. Tewari and T.K. Glasgow*
National Aeronautics and Space Administration
Lewis Research Center
Cleveland, Ohio 44135

SUMMARY

Hypoeutectic, eutectic, and hypereutectic nickel-molybdenum alloys have been rapidly solidified by both bulk undercooling and melt spinning techniques. Alloys were undercooled in both electromagnetic levitation and differential thermal analysis equipment. The rate of recalescence depended upon the degree of initial undercooling and the nature (faceted or nonfaceted) of the primary nucleating phase. Alloy melts were observed to undercool more in the presence of primary β (NiMo intermetallic) phase than in γ (fcc solid solution) phase. Melt spinning resulted in an extension of molybdenum solid solubility in γ nickel, from 28 to 37.5 at % Mo. Although the microstructures observed by undercooling and melt spinning were similar the microsegregation pattern across the γ dendrites was different. The range of microstructures evolved has been analysed in terms of the nature of the primary phase to nucleate, its subsequent dendritic growth, coarsening and fragmentation, and final solidification of interdendritic liquid.

INTRODUCTION

Rapid solidification of metallic alloys frequently results in extended solute solubility, greatly refined microstructures and formation of metastable phases. Chill block melt spinning is an attractive technique for production of thin ribbons which solidify with very high solid-liquid interface velocities (ref. 1). These high velocities are obtained by rapid heat extraction to the solid quench wheel. Large interface growth velocities are also obtained when the solid is allowed to grow in an undercooled alloy melt (ref. 2). The probability of heterogeneus nucleation at low undercoolings is reduced by using high purity elemental materials, maintaining purity during alloying, and by thermal conditioning of the melt in a suitable slag. When high degrees of undercoolings are attained initial solidification is rapid. Both the chill block melt spinning and bulk undercooling techniques are known to produce similar microstructural changes, such as reduced dendrite spacing (refs. 3 to 4), refined grain size (refs. 5 to 6), formation of metastable phases (ref. 7), particulate eutectics (refs. 8 to 9), extended solute solubility (refs. 8 and 10), etc. However, very little work has been reported where both the bulk undercooling and melt spinning techniques have been used to investigate and study microstructural and microchemical changes produced in the same binary alloy compositions. In this study hypoeutectic, eutectic, and hyper-eutectic nickel-molybdenum alloys have been rapidly solidified using the bulk undercooling and melt spinning techniques. Nickel-molybdenum binary alloys form the basis of some of the most important superalloys. This system is also

E-2751

attractive because it has a steep liquidus on the molybdenum rich side of the eutectic composition and a shallow liquidus on the nickel rich side (ref. 11). Differential thermal analysis and electromagnetic levitation techniques have been used to study the effect of alloy composition, level of initial undercooling, and nature of the solidifying phases on the microstructure obtained. Microsegregation across γ dendrites has been compared for the melt spun and undercooled alloys. Recalescence behavior after the nucleation of undercooled alloy specimens has been examined together with the resulting alloy microstructure. Melt spun foils have been examined for their range of microstructures produced across the ribbon thickness.

EXPERIMENTAL

Nickel (99.9 percent purity)-molybdenum (99.9 percent) charges with the alloy compositions marked on the Ni-Mo phase diagram (ref. 11) shown in fig. 1 were vacuum induction melted and investment cast to yield 1 cm diameter by 10 cm long alloy bars. Samples for undercooling and melt spinning were obtained from these cylinders machined to 6 mm diameter. Approximately 3 mm diameter alloy specimens were produced by thermal conditioning treatments carried out in a flowing argon atmosphere in a Pyrex/Vycor slag. These were then undercooled in a differential thermal analysis (DTA) unit at a cooling rate of 10 K/min, and solidified from various levels of undercoolings. The DTA furnace was switched off just after recording the final exothermic (solidification) peak. Through the courtesy of Prof. M.C. Flemings at Massachusetts Institute of Technology several thermally conditioned specimens were undercooled in an electromagnetic levitation (EML) unit. The specimen rested in a bed of Pyrex/Vycor powder in flowing argon. Directly coupled RF power which heated the specimen was turned off to cool the specimen. The specimen temperature was recorded by a two color optical pyrometer. The solidified specimens were metallographically examined and chemically analyzed by electron micro probe analysis.

The melt spun ribbons were cast by the free jet chill block melt spinning process in an apparatus described in ref. 12. A charge of about 20 g was heated to about 50 K above the liquidus temperature of the alloy and discharged in vacuum on to a 4340 steel wheel finished with 600 grit paper. The ejection pressure used was 8.6×10^4 N/m^2, the ejection hole was 1 mm in. diameter, and the wheel speed was 20 m/sec. Thin foils for TEM studies were made by electrochemical thinning using an alcohol/butyl cellusolve/perchloric acid mixture in a twin jet electropolishing equipment. Thin regions near the wheel side or the free surface were obtained by masking the other side using a lacquer.

RESULTS

Differential Thermal Analysis

Figure 2 shows the typical DTA plots obtained for the Ni-35 at % Mo eutectic alloy. Only one melting curve showing the eutectic temperature to be 1593 K is shown in this figure. At small undercoolings two exothermic peaks corresponding to two nucleation events were obtained. At greater undercoolings only one exothermic peak was observed. An examination of the nickel molybdenum phase diagram (fig. 1) shows that for an alloy of eutectic composition two

2

possibilities exist for the first phase to nucleate. It could be either nickel solid solution (γ) or intermetallic phase (β). Microstructural examination of the solidified specimens showed this behavior. The primary phase has been identified for the various DTA plots shown in fig. 2. The alloy melt can be seen to undercool in the presence of either the γ or β phase before the other phase nucleated. However, as the level of undercooling increased for nucleation of the primary phase, the extent of further melt undercooling for nucleation of the second phase decreased. Only one nucleation event was observed for the greatest levels of undercooling. Metallographic examination of the solidified specimens showed, however, that these specimens also had two nucleation events, which could not be distinguished from each other due to the insufficient response time of the DTA. The alloy melt was observed to undercool much more in the presence of primary "β" phase as compared to primary "γ" phase (fig. 2).

Figure 3 shows two typical types of microstructures observed in the eutectic alloy samples solidified in the DTA unit. For some of the specimens an orthogonal network of primary γ phase dendrites/or dendrite elements surrounded by γ-β eutectic was observed. The average spacing between these γ dendrite elements was observed to decrease with increasing undercooling, as has also been reported for other alloys (ref. 4). For other specimens the microstructure showed the evidence of primary β phase nucleating and growing in a "branched" manner in the melt before nucleation of the γ phase. The microstructure around the β dendrites consisted of nearly spherical γ dendrite elements surrounded by β phase.

Electromagnetic Levitation (EML)

Figure 4 shows typical thermal profiles obtained for the EML specimens. The raw temperature data obtained were quite noisy and had to be filtered in the manner described by Piccone (ref. 13) (filtered in both the directions, eight data points in each). The nucleation temperature (T_n) and the maximum recalescence temperature (T_m) are marked in this figure. The recalescence time is very small, a few milliseconds. The maximum racalescence temperature is approximately the same as the eutectic temperature for this specimen. The shape of the recalescence curve is sigmoidal, i.e., the rate of temperature rise goes through a maximum during recalescence. The recalescence time was observed to decrease with increasing undercooling, as has been reported for Ni-Sn alloys (ref. 13).

Figure 5 shows two typical microstructures obtained in the specimens solidified in the EML. One type of microstructure showed evidence of primary γ phase nucleating and growing in the melt in a fine dendritic manner, before solidification of rest of the melt. The microstructure consists of γ dendrite elements surrounded by either γ-β eutectic or β phase. The other showed evidence of primary β dendrites nucleating and growing in a nonorthogonal branched manner before rest of the alloy melt solidified. Both types of microstructures contain regions showing a "particulate eutectic" type of structure.

Figure 6 plots the maximum rate of temperature rise during recalescence measured from the thermal profiles for the hypoeutectic, eutectic and hypereutectic alloys, (similar to one shown in fig. 4) as a function of the initial level of undercooling (alloy liquidus-nucleation temperature). These

$\log(\delta T/\delta t)_{max}$ versus $\log(\Delta T)$ plots show a straight line fit with the slopes (m) as marked in the figure. The primary phase to nucleate and grow was γ for the hypoeutectic alloy, β for the hypereutectic alloy and either γ or β for the eutectic alloy. β did nucleate first for some hypoeutectic samples also. However, these have not been included in this figure.

Chill Block Melt Spinning

Two main features of the melt spun ribbon microstructures are shown in optical micrographs shown in figure 7. The alloys with molybdenum contents of 5, 17.5, and 28 at % showed a cellular/dendritic microstructure across the ribbon thickness. These cellular/dendritic features were identified to be due to nickel rich solid solution, fcc(γ) phase. The eutectic alloy (35 at % Mo) also showed these cellular/dendritic microstructures. In addition it showed a thin "featureless" region at optical microscopy resolution near the quench surface. This zone is not of uniform thickness along the ribbon length, most of the ribbon being occupied by the cellular/dendritic microstructure just described. Increasing molybdenum content of the alloy resulted in increased thickness of this "featureless" zone. This "featureless" zone was identified as the intermetallic, NiMo(β) phase for the eutectic alloy, and the β phase distributed in an amorphous matrix for the hypereutectic alloys.

Figure 8 shows the microstructure of γ phase in various regions of the eutectic alloy ribbon. The microstructure near the wheel surface (fig. 8(a)) consists of only γ grains. The linear features observed in this figure are due to the faulted nature of the supersaturated γ phase (ref. 14). There is no other phase observed in this region. The microstructure in the mid-ribbon portion consists of γ cells with the intercellular space occupied by β phase (fig. 8(b)). The free surface region of the ribbon has a dendritic microstructure, with the interdendritic regions occupied by β phase (fig. 8(c)). Note that the contrast within the cellular looking features due to the interdendritic β phase observed in the most slowly solidified regions of the ribbon (near free surface) is absent in the mid-ribbon region. This observation confirms that the γ in mid-ribbon region is cellular, whereas the γ near free surface region is dendritic.

Figure 9 shows the lattice parameter of the fcc nickel rich solid solution phase (γ) as a function of composition for the conventionally cast and rapidly solidified nickel-molybdenum alloys. For the conventionally cast material a linear increase in lattice parameter with increasing molybdenum content of the γ phase is observed up to 27.5 at % Mo. It remains constant beyond this molybdenum content, as would be expected from the Ni-Mo phase diagram, figure 1. A straight line fit up to the molybdenum content of 37.5 at % for the melt spun alloys observed from this figure shows that rapid solidification has resulted in extending the solute solubility from an equilibrium value of 28 to 37.5 at % Mo.

DISCUSSION

Bulk Undercooling Versus Solid-Liquid Interface Temperature Depression

As shown in figure 8 the microstructure across the ribbon thickness was not uniform. The fastest quenched region of eutectic alloy showed only grains

of γ phase in this micrograph. This region therefore must have solidified in a segregationless manner with a stable plane front liquid solid interface. This is possible because of the morphological stability associated with a very high liquid-solid interface velocity in this region (ref. 15). Such solidification is thermodynamically only possible at or below 'T_0', the temperature at which solid and liquid of the same composition have equal free energy (ref. 16. This observation suggests that solidification in this region occurred with the liquid-solid interface temperature depressed by at least 60 K (assuming that 'T_0' is located midway between the liquidus and solidus temperature). The observed extension of molybdenum solubility from the γ lattice parameter measurements (fig. 9) also suggests that melt spinning results in solidification occurring in the temperature regimes given by the extended liquidus-solidus.

The microstructure across most of the ribbon thickness however, is cellular/dendritic γ surrounded by β. The microstructure obtained from undercooled alloys, especially the one with the highest cooling rate after nucleation and larger bulk undercooling (e.g. fig. 5(a), EML specimen with undercooling, $\Delta T = 107$ K) also consists of γ dendrite elements surrounded by β. Rapid solidification by melt spinning and bulk undercooling therefore produces similar microstructures, except that the features are much finer for melt spun alloy. An examination of the microsegregation across the γ dendrites however, shows an important difference between melt spinning and bulk undercooling.

Figure 7 shows the microstructure and microsegregation across γ dendrites in a hypoeutectic alloy. Several solidification paths have been proposed for the solidification of an undercooled alloy melt (ref. 17). All of these suggest that the core of γ dendrite would be nickel poor: (First solid to form is of same composition as the melt. During recalescence the solid forming has same composition till either the solidus temperature or 'T_0' is reached. The subsequent solid forming follows the equilibrium solidus till the maximum recalescence temperature is reached. During subsequent cooling further formation of solid follows the solidus composition until the nucleation and growth of eutectic.) The solute profile in the undercooled specimen shows this nickel poor core, figure 10(a). However, the melt spun alloy shows the usual segregation pattern with a nickel rich core, figure 10(b). This observation suggests that the bulk melt puddle is not undercooled during melt spinning, but only the liquid-solid interface temperature is depressed due to curvature and large growth velocity effects. This observation is however, only strictly valid for the cellular/dendritic region of the melt spun foil. The fastest quenched region showed a segregationless solidification of the γ phase. For this region it is not possible to say whether the solidification occurred in an undercooled melt or not. A similar observation has been reported for a melt spun aluminum-copper alloy with a cellular microstructure (ref. 18).

Recalescence Behavior

For the EML specimens when the RF power is turned off the specimen cools until the solid nucleates. The latent heat released by rapid growth of the solid in the undercooled melt makes the specimen temperature rise sharply (fig. 4). At the beginning of the recalescence even though the dendritic growth rate is maximum due to the maximum undercooling in the liquid, the area

5

of the liquid-solid interface is also small. This results in a low rate of solid formation and low rate of temperature rise. As the specimen temperature rises during further recalescence the dendritic growth rate decreases but the liquid-solid interfacial area is greater, resulting in a higher rate of temperature rise. Near the end of recalescence the dendritic growth speed due to the low level of undercooling is least. Such effects should cause the sigmoidal appearance of the recalescence behavior (fig. 4). The technique of data filtering (eight data points in each direction, ref. 13) can however, also lead to such a sigmoidal appearance; especially when there are only a small number of data points available during the recalescence.

The temperature sensed by the pyrometers is expected to be a complex function of the specimen size, thermal properties of the undercooled liquid and solid, Pyrex/Vycor environment, undercooling, nature of the growing phase/phases, etc. A rigorous theoretical understanding of the recalescence behavior is therefore very nearly impossible. In order to make some sense from these recalescence data we would make some crude assumptions. Let us assume that the growth rate, R, is proportional to the maximum rate of temperature rise ($\delta T/\delta t_{max}$) observed during the recalescence and that this growth rate corresponds to the initial level of undercooling, ΔT. The dendritic growth speed in an undercooled melt is known to increase with the increasing degree of undercooling in a manner described by, $R(\Delta T)^m$, with the m value between 1.8 to 3 (ref. 2). A plot of $\log(\delta T/\delta t)_{max}$ versus $\log(\Delta T)$ would therefore be expected to give rise to a straight line fit with a slope equal to m. Based on the limited sets of data in figure 6 such a straight line fit is observed. This figure gives m equal to 8.6 for the γ dendrites growing as compared to only 2.9 for the β dendrites. The NiMo (β) phase is a faceting type and its growth is expected to be controlled by the solute attachment kinetics. The β phase is therefore expected to grow less rapidly than γ, a nonfaceting phase, for which solute diffusion in the liquid is expected to control the growth rate. This results in a steeper dependence of $(\delta T/\delta t)_{max}$ on ΔT for the γ phase growth as compared to the β phase growth.

Microstructural examination of the melt spun foils also shows that even at the relatively high heat extraction rates encountered during melt spinning the γ phase grows with a much faster growth velocity than β phase. Figure 7(b) shows that the γ phase nucleating on the wheel surface grows much faster than the β phase nucleating on the wheel surface. The gamma phase also spreads laterally much faster. As a result only γ dendrites are observed in most of the eutectic alloy ribbon.

It is also interesting to compare the γ grain sizes for the 28.0 at % Mo alloy near the chill surface with those γ grains nucleated on the β surface in the 35.0 at % Mo alloy (fig. 7(b)). The grain size for γ grains nucleating in contact with β phase is much larger than those nucleating in contact with the chill block. As shown in figure 2 the β phase has been shown to be a poor nucleant for γ in nickel-molybdenum alloy melt, resulting in considerable undercooling of the alloy melt in the presence of β dendrites. The nucleation rate of the λ phase for the same melt temperature is therefore expected to be lower, when it nucleates in contact with β phase, as compared to when it nucleates in contact with the wheel surface. This lower nucleation frequency explains the above mentioned grain size variation.

Microstructural Evolution

Figure 11 shows the range of microstructures obtained in the nickel-molybdenum eutectic alloy for various undercoolings and solidification conditions. It also shows schematically the mechanisms responsible for producing these microstructures. As explained earlier either the γ or the β phase can nucleate first from the alloy melt. The solid-liquid interface growing in an undercooled alloy melt is inherently unstable and prone to dendritic breakdown unless the growth velocity exceeds the "absolute stability" limit of Mullins and Sekerka (ref. 15). A dendritic network of either γ(orthogonal) or β(nonorthogonal) therefore immediately forms in the melt. During subsequent solidification this network grows, coarsens, fragments and the other phase nucleates and grows. If the first phase to nucleate is γ, two types of microstructures result. If the local solidification conditions are such that the interdendritic spacing is of the same order as interlamelar spacing of the eutectic, a "particulate eutectic" microstructure results, in which γ dendrite elements are surrounded by β phase (fig. 11(a)). Otherwise the γ interdendritic region is occupied by γ-β eutectic (fig. 11(b)). If the first phase to nucleate is β, three types of microstructures can evolve. Large undercoolings would prevent coarsening of the β dendritic network. The γ phase nucleating subsequently in the β interdendritic regions would produce a "complex regular" type of microstructure which consists of fine β dendritic skeletons on which γ-β "eutectic like" microstructure has formed (fig. 11(c)). For a lesser degree of undercooling in which the β dendritic network achieves some coarsening and it also undergoes fragmentation of its network before the γ phase nucleates in the interdendritic regions, the microstructure shown in figure 11(d) would evolve. This microstructure would contain uniformly distributed γ and β phases ("particulate eutectic"). In case the β phase nucleates first and has time to coarsen and agglomorate considerably before the nucleation of the γ phase, a microstructure shown in figure 11(e) would be expected to result.

CONCLUSIONS

Nickel-molybdenum binary alloys of hypoeutectic, eutectic and hypereutectic compositions have been rapidly solidified using bulk undercooling by both differential thermal analysis and electromagnetic levitation and by chill block melt spinning techniques. The following conclusions can be drawn from this study,

1. DTA specimens showed two nucleation events for solidification of the undercooled alloy melt corresponding to nucleation of either supersaturated γ(fcc) or hypostoichiometric β(NiMo). The melt showed considerable further undercooling in the presence of either γ or β dendrites. The undercooling was however, much greater in the presence of β dendrites.

2. The maximum rate of temperature rise $(\delta T/\delta t)_{max}$ during recalescence for the EML specimens has the following dependence on the initial level of undercooling (ΔT),

$$(\delta T/\delta t)_{max} \, \alpha (\Delta T)^m,$$

the value of m being 8.6 for the γ dendritic network growth and 2.9 for the β dendritic growth. The faceted phase $(\beta, NiMo)$ grows at slower rate as

7

compared to the nonfaceted phase (γ,fcc Ni solid solution) even at the very rapid rates of heat extraction encountered in melt spinning.

3. Melt spinning resulted in extending molybdenum solid solubility from a maximum equilibrium value of 28 to 37.5 at %. Rapid solidification by melt spinning does not cause solidification in an undercooled melt puddle. The liquid-solid interface temperature however, may be considerably depressed, as much as 60 K for the eutectic alloy.

4. The nucleation frequency during melt spinning of the molybdenum supersaturated γ grains is much lower in contact with the β phase as compared to that in contact with the wheel surface.

5. A range of microstructures can be formed by solidification of under-cooled Ni-Mo alloys. These evolve due to nucleation and growth of dendritic network of either the γ phase (orthogonal network) or β phase (nonortho-gonal network) first in the melt and subsequent nucleation and growth of the other phase in the interdendritic regions. When recalescence is sufficient, the particulate eutectic is one such microstructure.

ACKNOWLEDGEMENT

REFERENCES

1. S.C. Huang, R.P. Laforce, A.M. Ritter, and R.P. Goehner: Metall. Trans. A, 1985, vol. 16A, pp. 1773-1779.

2. K. Kobayashi, M.I. Kumikawa, and P.H. Shingu: J. Crystal Growth, 1984, vol. 67, pp. 85-90.

3. H.A. Davies, N. Shoji, and D.H. Warrington: in Rapid Solidification Processing: Principles and Technologies, R. Mehrabian, B.H. Kear, and M.Cohen, eds., pp. 153-164, Claitor's Publishing Division, Baton Rouge, LA, 1980.

4. T.Z. Kattamis and M.C. Flemings: Mod. Cast., 1967, vol. 52, pp. 97-104.

5. P.G. Boswell and G.A. Chadwick: Scripta Metall., 1977, vol. 11, pp. 459-465.

6. T.Z. Kattamis: in Fundamentals of Alloy Solidification Applied to Industrial Processes, NASA CP-2337, pp. 15-32, National Aeronautics and Space Administration, 1984.

7. D. Turnbull: Metall. Trans. B, 1981, vol. 12B, pp. 217-230.

8. R. Cheese and B. Cantor: <u>Mater. Sci. Eng.</u>, 1980, vol. 45, pp. 83-93.

9. K.P. Cooper, I.E. Anderson, and J.H. Perepezko: <u>Rapidly Quenched Metals IV</u>, vol. 1, T. Masumoto and K. Suzuki, eds., pp. 107-110, The Japan Institute of Metals, Sendai, Japan, 1982.

10. M.G. Chu, Y. Shiohara, and M.C. Flemings: <u>Metall. Trans. A</u>, 1984, vol. 15A, pp. 1303-1310.

11. <u>Metals Handbook</u>, vol. 8, p. 319, American Society for Metals, Metals Park, OH, 1973.

12. R.W. Jech, T.J. Moore, T.K. Glasgow, and N.W. Orth: <u>J. Met.</u>, 1984, vol. 36, no. 4, pp. 41-45.

13. T.J. Piccone: Thermal History and Microstructure of Undercooled Nickel-Tin Alloys, M.S. Thesis, Massachusetts Institute of Technology, Sept. 1984.

14. N. Jayaraman and S.N. Tewari: "Fault Structures in Rapidly Quenched Ni-Mo Binary Alloys," (submitted to Metall. Trans.).

15. W.W. Mullins and R.F. Sekerka: <u>J. Appl. Phys.</u>, 1964, vol. 35, pp. 441.

16. J.C. Baker and J.W. Cahn: <u>Acta Metall.</u>, 1969, vol. 17, pp. 575-578.

17. T.Z. Kattamis: Z. Metallkunde, 1970, vol. 61, pp. 856-860.

18. L.J. Masur and M.C. Flemings: <u>Rapidly Quenched Metals IV</u>, vol. 2, T. Masumoto and K. Suzuki, eds., pp. 1557-1560, The Japan Institute of Metals, Sendai, Japan, 1982.
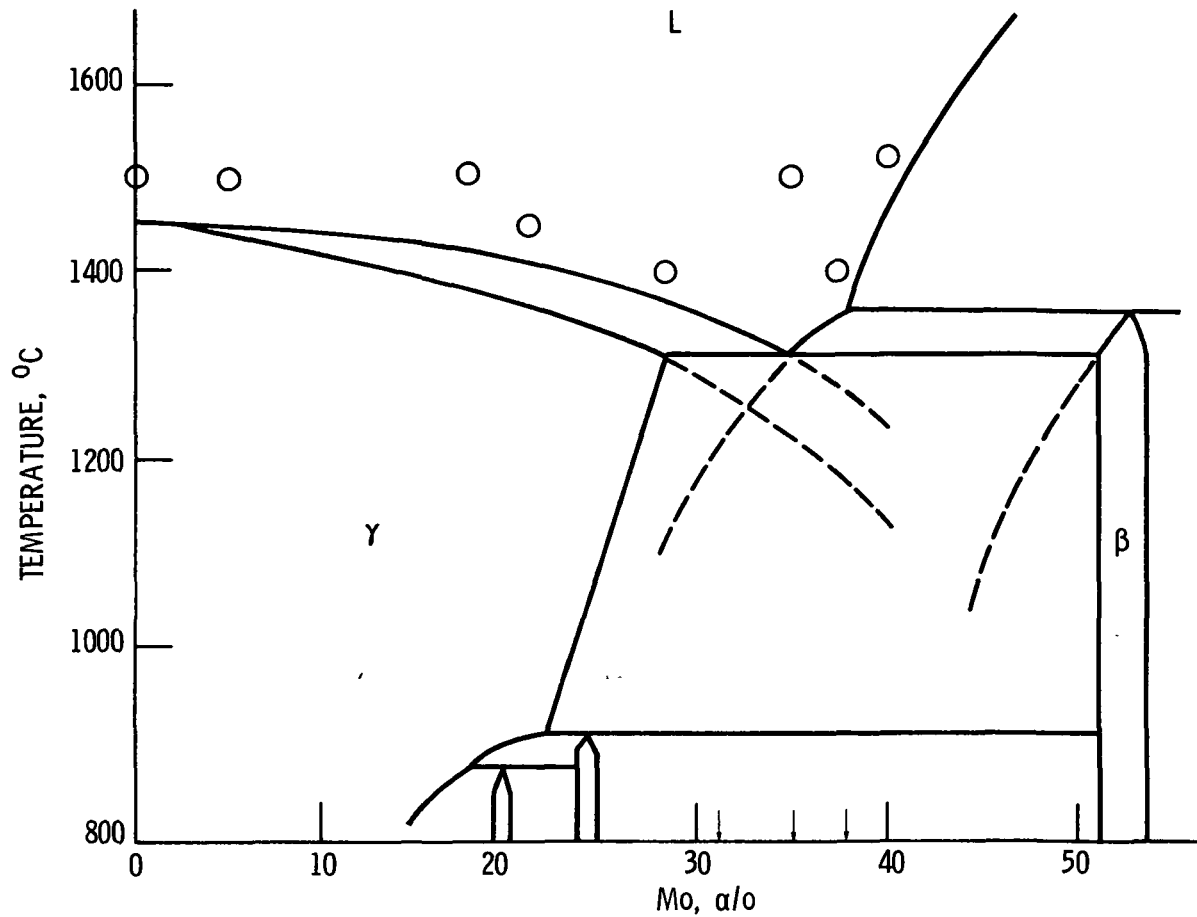
Figure 1. - Nickel-molybdenum phase diagram. ○ shows the compositions and
melt temperatures for the Chill Block Melt Spun ribbons. ↓ shows the com-
positions solidified by bulk undercooling.
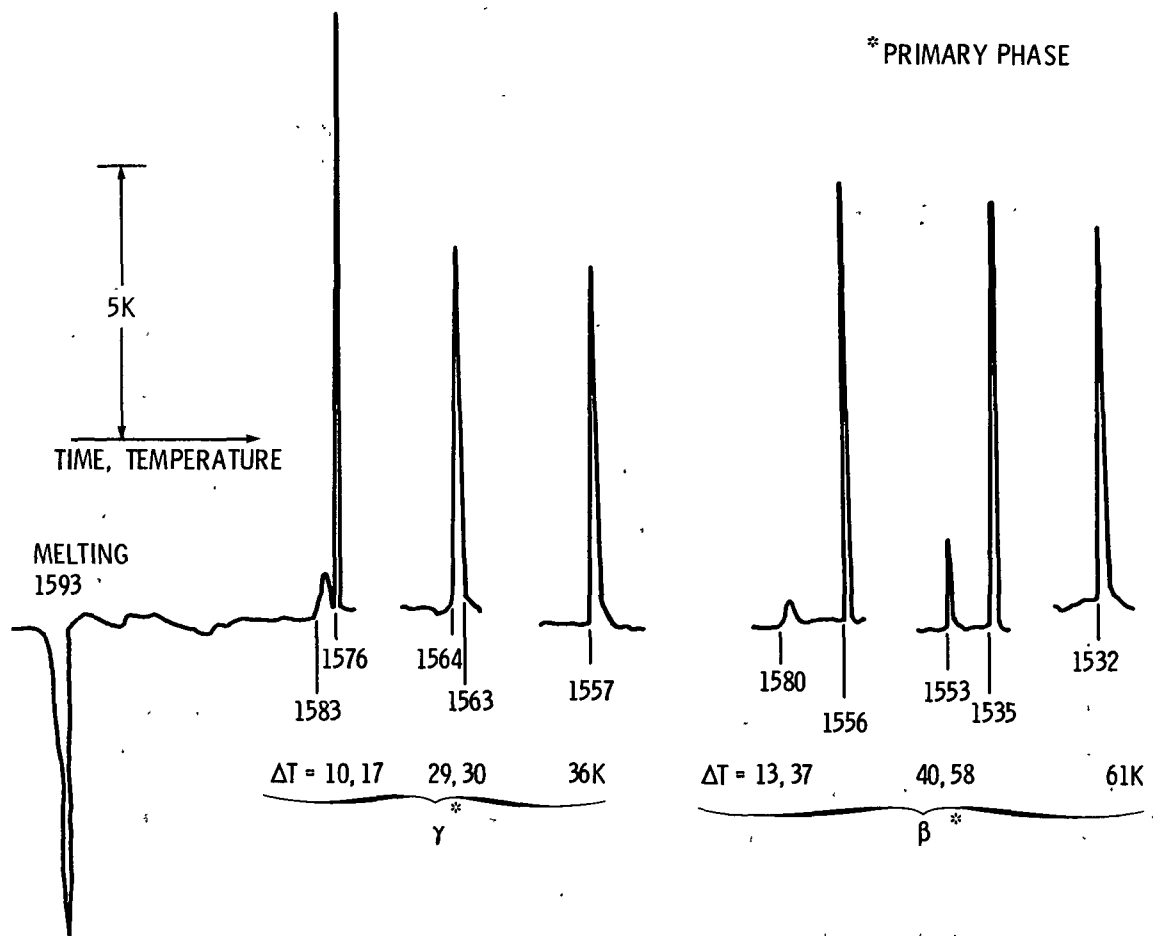
Figure 2. – Differential thermal analysis (DTA) plots for eutectic Ni-Mo alloy.
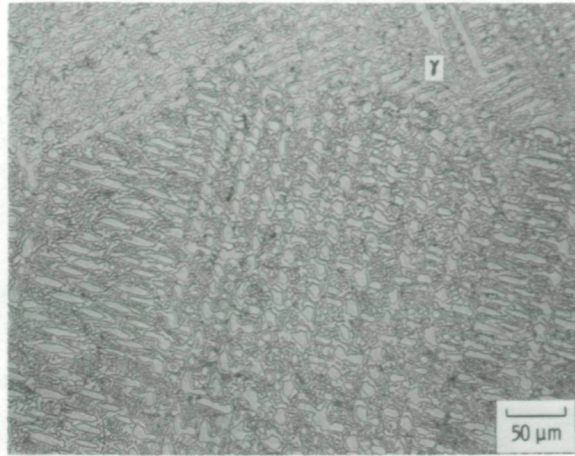
(a) $\triangle T$ = 36 K. first phase to nucleate and
grow is γ.
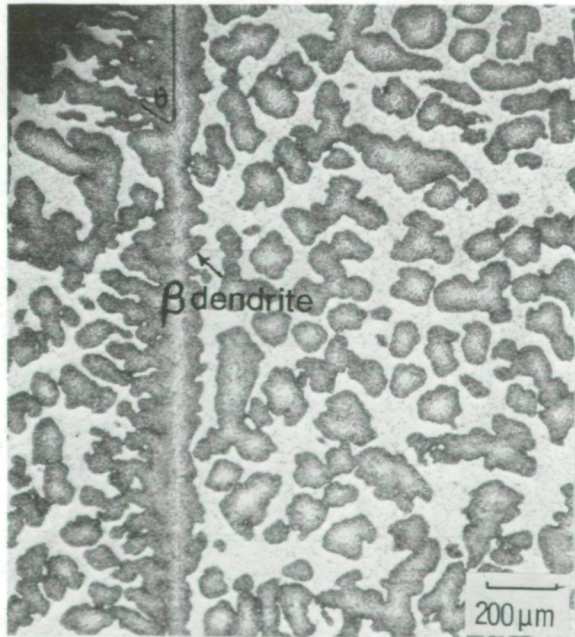
(b) $\triangle T$ = 114 K, first phase to nucleate and
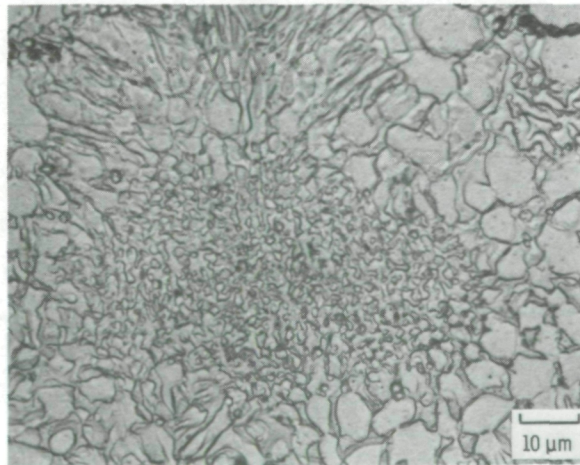grow is β.

Figure 3. - Microstructure of eutectic alloy
solidified in DTA.

(a) Raw temperature data.

(b) Filtered temperature data.
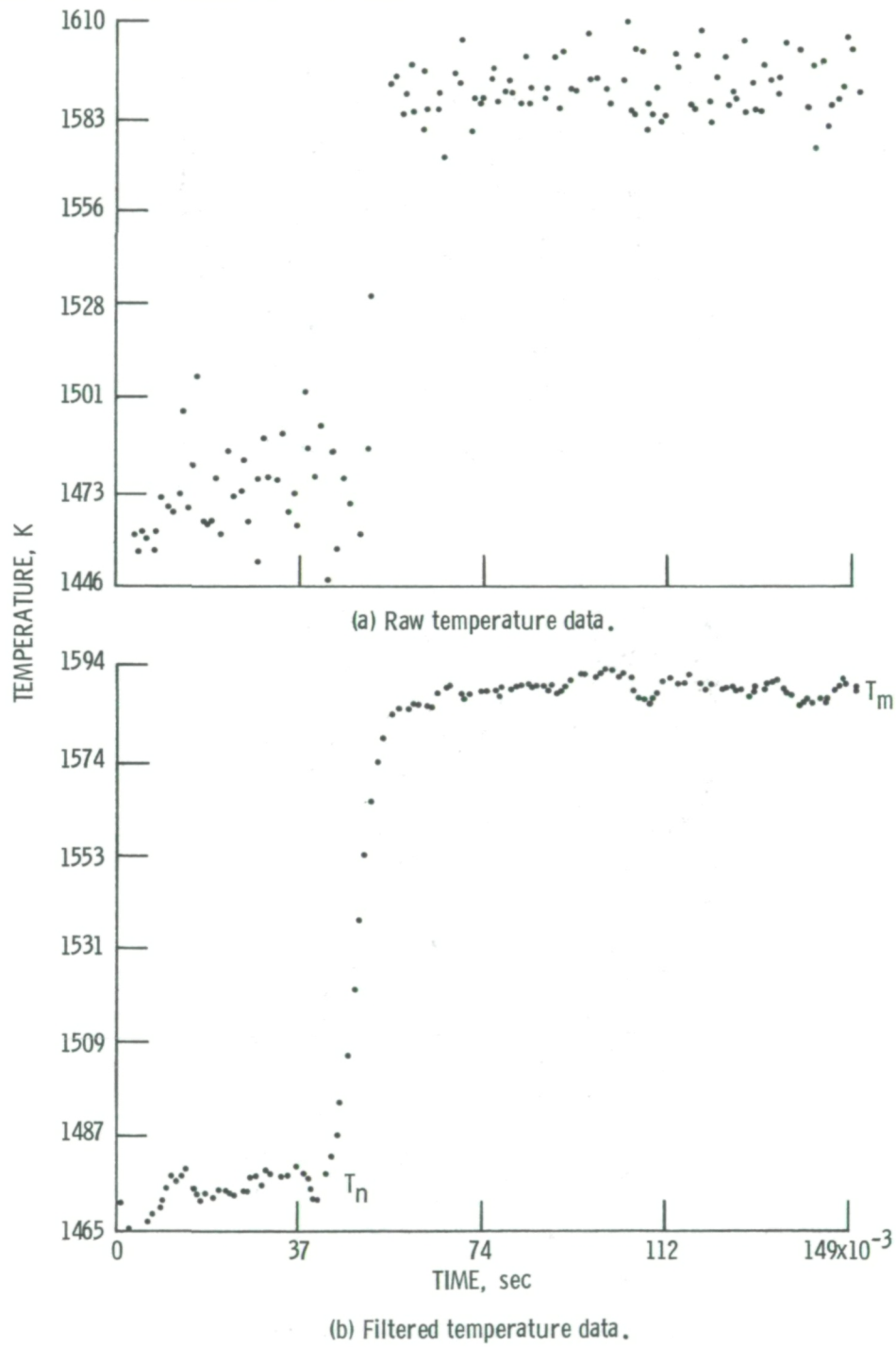
Figure 4. - Typical recalescence behaviour for eutectic alloy solidified from an undercooling (ΔT) of 160 K.
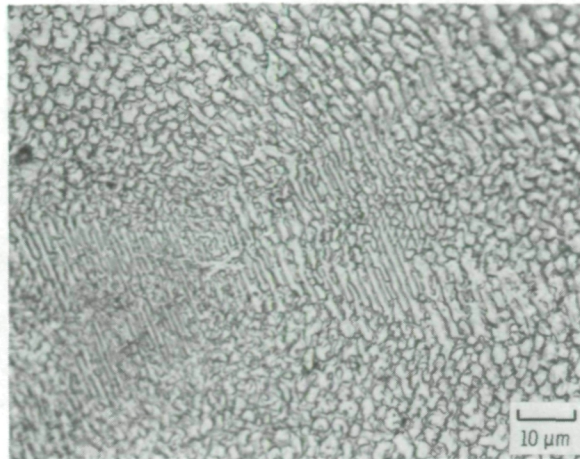
(a) ΔT = 107 K, first phase to nucleate and grow in the melt is γ.

(b) ΔT = 58 K, first phase to nucleate and grow in the alloy melt is β.

Figure 5. - Microstructure of eutectic alloy (Ni-35 at % Mo) solidified in electromagnetic levitation unit.
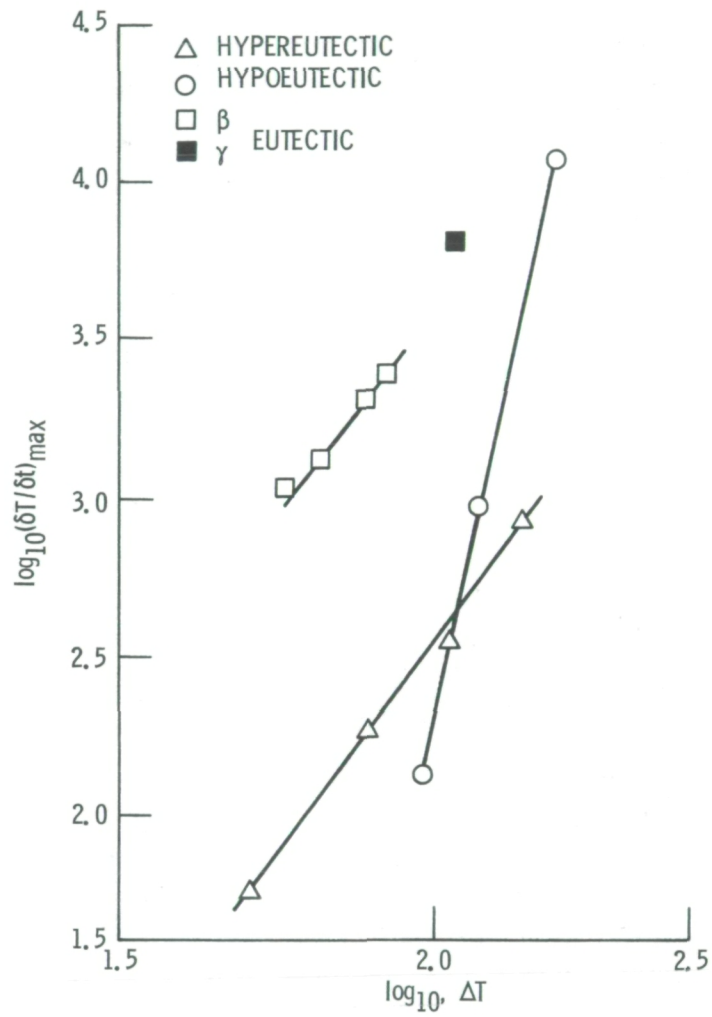
Figure 6. - Dependence of the maximum rate of temperature rise during recalescence $(\delta T/\delta t)$ max on the initial level of undercooling (ΔT).
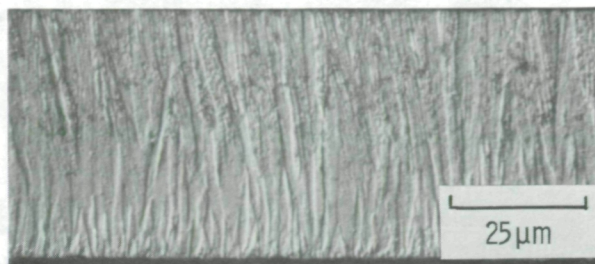
(a) 28.0 at % Mo.
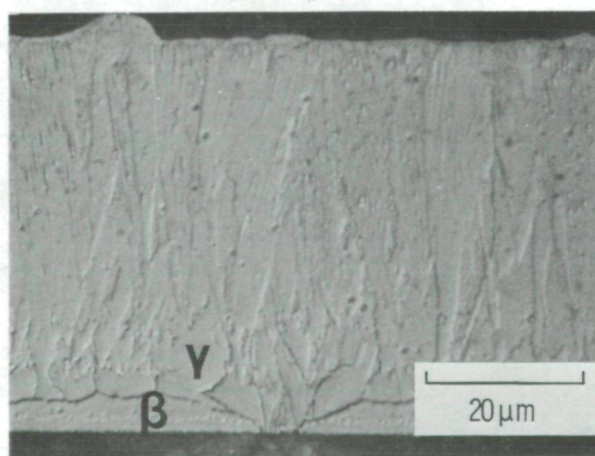
(b) 35.0 at % Mo.

Figure 7. - Microstructure across the chill block spun ribbons of nickel-molybdenum alloys.
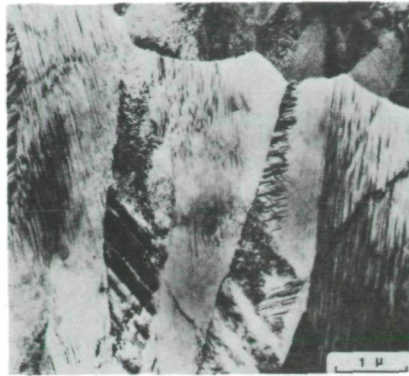
(a) Near the quench wheel surface.
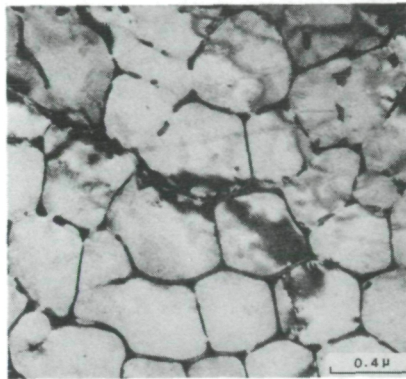
(b) Mid foil thickness.
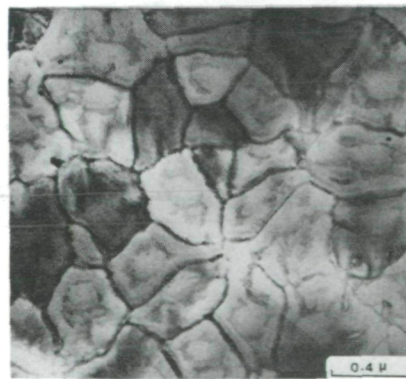
(c) Near the free surface.

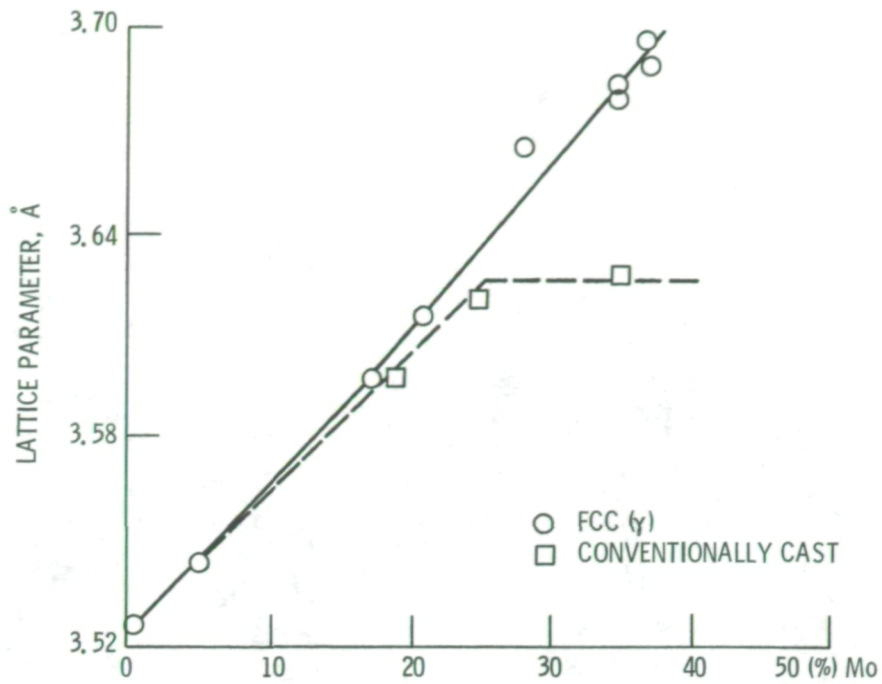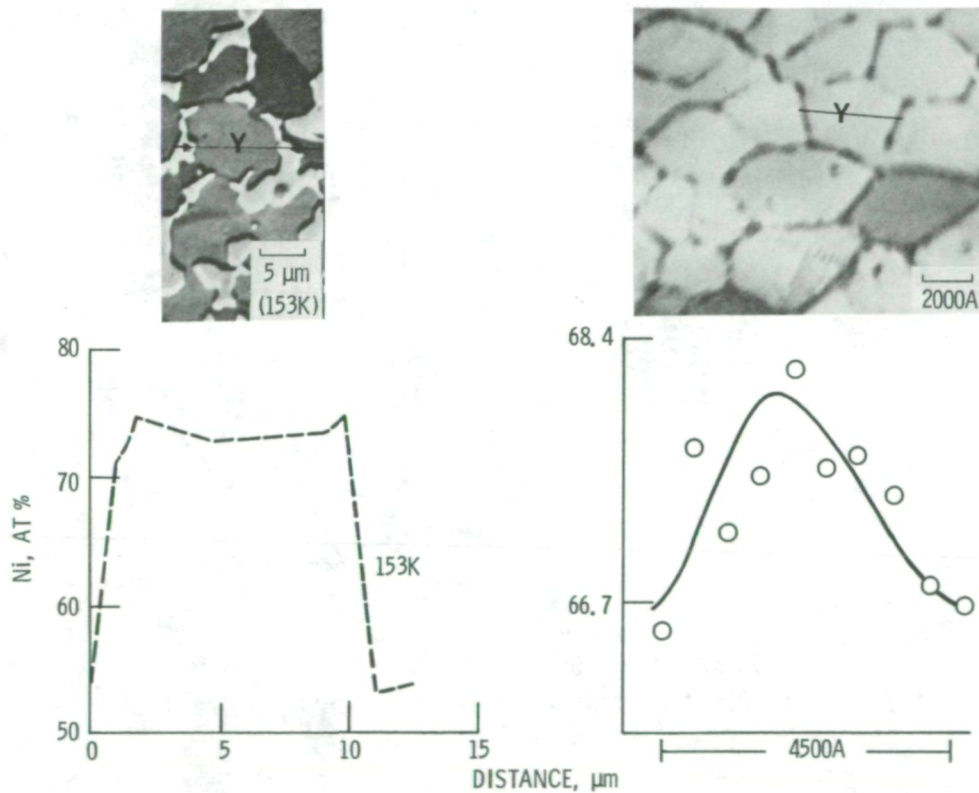Figure 8. - Microstructure of γ phase formed in various regions of melt spun eutectic alloy ribbon.

Figure 9. - Lattice parameter of the FCC Nickel γ phase as /a function of composition in conventionally cast and rapidly solidified Ni-Mo alloys.

(a) From an undercooling of 153 K (DTA).

(b) Chill block melt spun alloy.

Figure 10. - Microstructure and microsegregation in solidified hypoeutectic alloy (Ni-31 at % Mo).
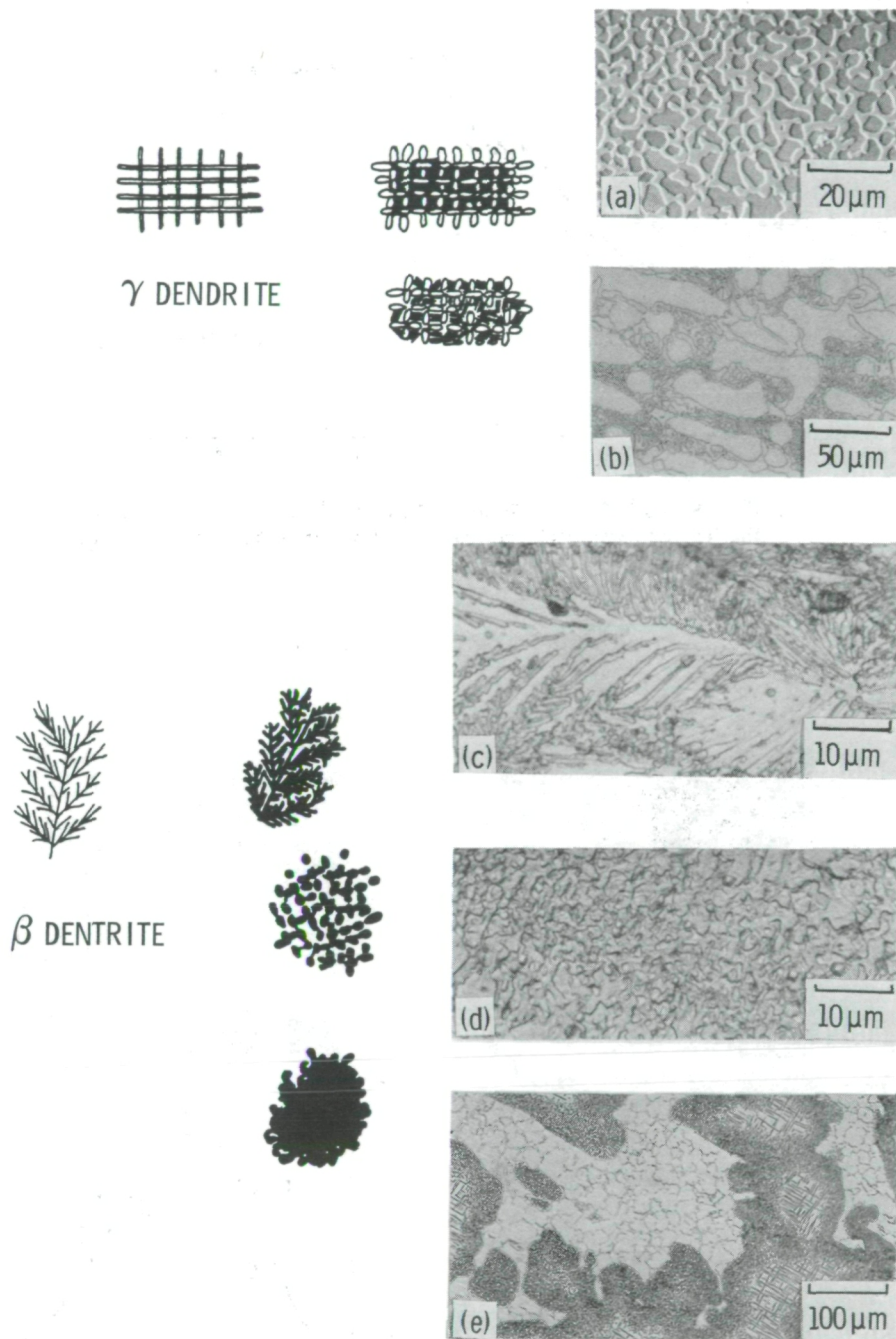
γ DENDRITE

β DENTRITE

(a) 20 μm

(b) 50 μm

(c) 10 μm

(d) 10 μm

(e) 100 μm

Figure 11. - Range of microstructures formed by solidification
of eutectic alloy from an undercooled melt and their evolution.
The dark phase in the schematic representations is β.

1. Report No. NASA TM-87257	2. Government Accession No.	3. Recipient's Catalog No.
4. Title and Subtitle Undercooled and Rapidly Quenched Ni-Mo Alloys		5. Report Date
		6. Performing Organization Code 674-25-05
7. Author(s) S.N. Tewari and T.K. Glasgow		8. Performing Organization Report No. E-2947
		10. Work Unit No.
9. Performing Organization Name and Address National Aeronautics and Space Administration Lewis Research Center Cleveland, Ohio 44135		11. Contract or Grant No.
		13. Type of Report and Period Covered Technical Memorandum
12. Sponsoring Agency Name and Address National Aeronautics and Space Administration Washington, D.C. 20546		14. Sponsoring Agency Code

15. Supplementary Notes

16. Abstract

Hypoeutectic, eutectic, and hypereutectic nickel-molybdenum alloys have been rapidly solidified by both bulk undercooling and melt spinning techniques. Alloys were undercooled in both electromagnetic levitation and differential thermal analysis equipment. The rate of recalescence depended upon the degree of initial undercooling and the nature (faceted or nonfaceted) of the primary nucleacting phase. Alloy melts were observed to undercool more in the presence of primary β (NiMo intermetallic) phase than in γ (fcc solid solution) phase. Melt spinning resulted in an extension of molybdenum solid solubility in γ nickel, from 28 to 37.5 at % Mo. Although the microstructures observed by undercooling and melt spinning were similar the microsegregation pattern across the γ dendrites was different. The range of microstructures evolved has been analysed in terms of the nature of the primary phase to nucleate, its subsequent dendritic growth, coarsening and fragmentation, and final solidification of interdendritic liquid.

17. Key Words (Suggested by Author(s)) Rapid quenching; Undercooling; Nickel molybdenum; Rapid solidification	18. Distribution Statement Unclassified - unlimited STAR Category 26
19. Security Classif. (of this report) Unclassified	20. Security Classif. (of this page) Unclassified	21. No. of pages	22. Price*

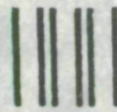SECOND CLASS MAIL

ADDRESS CORRECTION REQUESTED

NASA